Dimensional analysis and centrifuge modeling of quay wall of large-diameter bottomless cylinders

XU Guang-ming[1], NG C W W[2]

(1. Nanjing Hydraulic Research Institute, Nanjiing 210029, China; 2. Hong Kong University of Science and Technology, Hong Kong, China)

Abstract: Understanding the interaction mechanism between the soil and a quay wall composed of large-diameter bottomless cylinders is vital to the safe and economic design of the quay wall. Based on dimensional analysis, a number of dimensionless groups that governed the performance of the quay wall were investigated, identified and used to design and interpret centrifuge model tests. In all centrifuge model tests performed, a deformation mechanism was observed, that is, the upper part of the wall tilted outward away from the retained soil, and the ground behind it settled. Based on multi-regression analysis of the centrifuge test results, it was found that the horizontal displacement of the wall/cylinder was most sensitive to the ratio of embedded soil depth in front of the cylinder to the height of the cylinder and it was 50% less sensitive to the ratio of the diameter to the height of the cylinder. Relatively the measured deformation and lateral earth pressure were insensitive to the roughness of the wall. Lateral earth pressures acting on the wall could be predicted from the Rankine active earth pressure theory with the undrained assumption in the short term.

Key words: soil and structure interaction; large-diameter cylinder; embedded quay wall; dimensional analysis; multiple regression analysis

CLC number: TU47 **Document code**: A **Article ID**: 1000－4548(2007)10－1544－09

Biography: XU Guang-ming (1963－), male, Prof. of Geotechnical Engineering Department, Nanjing Hydraulic Research Institute, Nanjing, P.R. China. E-mail: gmxu@nhri.cn.

大圆筒岸壁码头的量纲分析和离心模拟

徐光明[1]，吴宏伟[2]

(1. 南京水利科学研究院，江苏 南京 210029；2. 香港科技大学，香港)

摘 要：认识土与沉入式无底大直径圆筒结构岸壁码头之间相互作用机制，对于它的安全和经济设计至关重要。基于量纲分析，首先研究确定了控制这种岸壁码头性状的无量纲项，然后，为研究这些无量纲项的相对重要性，设计了模型试验，并对试验结果分析解释。在所完成的离心模型试验中，就岸壁码头变形机制进行了观察，发现圆筒岸壁上部是偏离墙后土体向海侧倾斜，同时码头后场表面有沉降发生。离心试验结果的多元回归分析发现，圆筒岸壁的相对侧向位移对筒体前侧嵌入泥面以下的埋深比最为敏感，而侧向位移对圆筒的径高比的灵敏度不足前一因素的50%。相对来说，所测得的位移和土压力对筒壁的摩擦不很灵敏。对土压力结果的分析表明，作用于圆筒岸壁的侧向土压力可依据朗肯主动土压力理论，根据筒后土体的不排水强度进行预测。

关键词：土与结构相互作用；大直径圆筒；沉入式岸壁码头；量纲分析；多元回归分析

0 Introduction

With the development in material science and construction technologies, quay-wall structures have been continuously innovated and modified over the last several decades. In port and harbour engineering, gravity-type caisson walls have become popular due to the development in prefabricated concrete structural members. The forms of such caissons have evolved from simple cubical boxes to more complicated but more economical and efficient shapes such as cylinders with closed-end bottoms to retain water and earth pressures. Bottomless cylinders have also been developed for the construction of quay walls. The deep-water quay wall built in LeHavre, France in the mid-1950s was among the world's first major quay walls successfully constructed from large-diameter concrete cylinders

Received date：2006－09－12

(Tsinker, 1997). Depending on ground conditions, bottomless concrete cylinders may be placed on a well-prepared rubble mattress or sunk into the foundation soil within a shallow depth underneath the seafloor. In the case of the latter construction, the in-situ soil within the cylinders is usually excavated and then replaced by granular materials (Tsinker, 1997).

Recently, a relatively new attempt has been made to use large-diameter cylinders in the construction of a deep-water port founded on thick soft soil deposits (Zhou & Liu, 1995). This application uses in-situ soft soil as the back fill material inside the cylinders. Subsequently, the shear strength of the fill material is improved by installing vertical drains and by pre-loading. In this way, underwater dredging and back filling can be minimised or even avoided, leading to substantial savings.

Generally, quay walls formed by cylinders are considered to be gravity structures when the ratio of the cylinder diameter (D) to its height (H) exceeds 0.7 and it is embedded into the foundation soil less than 0.2H deep (Tsinker, 1997). This type of structure develops its lateral and overturning resistance primarily from its own body weight and the passive earth pressure in front of the wall. Compared with quay walls founded on rubble mattresses (Liu, 1994), the performance of a gravity quay wall founded in soil with a shallow penetration depth is not fully understood. Moreover, the influence of the D/H ratio, embedded depth in front of the wall (h) and any contributions of interface friction between the soil and the wall on the stability and deformation of the wall need carefully investigations in order to improve our understanding and to optimise the design of this type of gravity quay wall. In this paper, the stability and deformation mechanism of a gravity-type reinforced concrete quay wall made of large-diameter bottomless cylinders are studied using dimensional analysis (DA) and investigated by conducting a series of centrifuge model tests. The relative importance of the governing factors of the stability and deformation mechanism of the quay wall is investigated through multiple regression analysis.

1 Dimensional analysis

As pointed out by Sedov (1993), dimensional analysis can be used to investigate phenomena or mechanisms that depend on a great number of variables. Fig. 1 depicts the variables or physical quantities that may be relevant to the performance of reinforced concrete quay walls made of large-diameter bottomless cylinders sunk into a foundation soil. For a specific system, the physical quantities may be grouped into one set of independent variables and another set of dependent ones. The independent variables refer to the internal fundamental properties of the system (e.g., the physical-mechanical parameters of material) and external boundary conditions (e.g., the external load conditions or displacement constraint conditions), whereas the dependent variables refer to those that can characterise the response of the system to external boundary conditions, such as the distribution of deformation, displacement, and stress within the system.

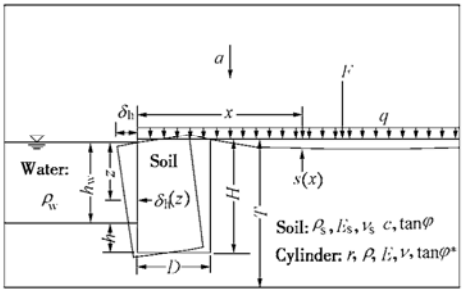

Fig. 1 Schematic interaction of submerged quay wall

Following the procedures proposed by Butterfield (1999), the dimensional analysis is carried out to establish general functional relations of dependent variables to their relevant independent variables. For the case shown in Fig. 1, the dependent variable of interest is the short-term deformation of the large-diameter cylindrical quay wall. For the sake of clarity, three simplifications have to be made. First, only one single uniform soil layer is considered and, second, the soil is linear elastic and hence its deformation is governed by Young's modulus (E_s) and Poisson's ratio (ν_s). Finally, the depth of the water is assumed to be constant.

To characterize the behavior of the quay wall, three dependent variables are identified: horizontal displacement (δ_h) at the top of the cylinder, any settlement, $s(x)$, at distance x from the quay wall and lateral earth pressure at any depth z, $\sigma_h(z)$, acting on the back wall. A summary of all dependent and independent variables identified together with the dimensionless groups is given in Table 1. The horizontal displacement, δ_h, at the top of the wall, is considered to be dependent on 18 independent variables. Thus, a total of 19 variables

are required for DA.

$$V=\left\{\delta_{\mathrm{h}},H,D,h,t,\rho,E,\nu,T,\rho_{\mathrm{s}},E_{\mathrm{s}},\nu_{\mathrm{s}},c,\tan\varphi,\rho_{\mathrm{w}},\tan\varphi^{*},a,q,F\right\} \tag{1}$$

Table 1 shows that 3 primary dimensions: {*M*, *L*, *T*} are necessary and sufficient to define all components of *V* (Butterfield, 1999). Thus, 16 (i.e., 19-3) DGs can be compiled. By adopting {ρ_{s}, *a*, *H*} as 'repeated' variables, the remaining 'isolated' variables (Butterfield, 1999) are $\left\{\delta_{\mathrm{h}},H,D,h,t,\rho,E,\nu,T,\rho_{\mathrm{s}},E_{\mathrm{s}},\nu_{\mathrm{s}},c,\tan\varphi,\rho_{\mathrm{w}},\tan\varphi^{*},a,q,F\right\}$. These 16 DGs can be compiled. They are {δ_{h}/H, D/H, h/H, t/H, ρ/ρ_{s}, $E/(\rho_{\mathrm{s}}aH)$, ν, T/H, $E_{\mathrm{s}}/(\rho_{\mathrm{s}}aH)$, ν_{s}, $c/(\rho_{\mathrm{s}}aH)$, $\tan\varphi$, $\rho_{\mathrm{w}}/\rho_{\mathrm{s}}$, $\tan\varphi^{*}$, $q/(\rho_{\mathrm{s}}aH)$, $F/(\rho_{\mathrm{s}}aH^{2})$}, as given in Table 1. Therefore, the dependent variable, (δ_{h}/H), can be expressed as a function of the remaining 15 independent DGs as follows:

$$\begin{aligned}\delta_{\mathrm{h}}=H=\Phi_{1}\{&D/H,h/H,t/H,\rho/\rho_{\mathrm{s}},\\&E/(\rho_{\mathrm{s}}aH),\nu,T/H,E_{\mathrm{s}}/(\rho_{\mathrm{s}}aH),\nu_{\mathrm{s}},c/(\rho_{\mathrm{s}}aH),\\&\tan\varphi,\rho_{w}/\rho_{s},\tan\varphi^{*},q/(\rho_{\mathrm{s}}aH),F/(\rho_{\mathrm{s}}aH)\}\end{aligned} \tag{2a}$$

As the horizontal displacement at any arbitrary depth is often of interest, z can be introduced as a variable in V. By adding a DG, z/H, a more general relationship of $\delta_{\mathrm{h}}(z)/H$ and its possible independent variables can be derived and written as follows:

$$\begin{aligned}\delta_{\mathrm{h}}(z)/H=\Phi_{2}\{&D/H,h/H,t/H,\rho/\rho_{\mathrm{s}},E/(\rho_{\mathrm{s}}aH),\\&\nu,T/H,E_{\mathrm{s}}/(\rho_{\mathrm{s}}aH),\nu_{\mathrm{s}},c/(\rho_{\mathrm{s}}aH),\tan\varphi,\\&\rho_{w}/\rho_{s},\tan\varphi^{*},q/(\rho_{\mathrm{s}}aH),F/(\rho_{\mathrm{s}}aH)\},z/H\end{aligned} \tag{2b}$$

Similarly, the surface settlement, $s(x)$, at any distance, x, from the front face of the wall can also be related to its independent variables as follows:

$$\begin{aligned}s(x)/H=\Phi_{3}\{&D/H,h/H,t/H,\rho/\rho_{\mathrm{s}},E/(\rho_{\mathrm{s}}aH),\\&\nu,T/H,E_{\mathrm{s}}/(\rho_{\mathrm{s}}aH),\nu_{\mathrm{s}},c/(\rho_{\mathrm{s}}aH),\tan\varphi,\\&\rho_{\mathrm{w}}/\rho_{\mathrm{s}},\tan\varphi^{*},q/(\rho_{\mathrm{s}}aH),F/(\rho_{\mathrm{s}}aH)\},x/H\end{aligned} \tag{3}$$

Table 1 Sets of variables, repeated variables and dimensionless groups for the quay wall

	Name of variable (V)	Symbol	Dimension	Dimensionless Group (DG)
Dependent variables	Horizontal displacement at the top, or at any arbitrary depth z, of the quay wall, δ_{h} and $\delta_{\mathrm{h}}(z)$, respectively	δ_{h}; $\delta_{\mathrm{h}}(z)$.	L	δ_{h}/H; $\delta_{\mathrm{h}}(z)/H$
	Settlement at any distance, x, behind the front face of the quay	$s(x)$	L	$s(x)/H$
	Earth pressure acting at any depth, z, behind the wall	$\sigma_{\mathrm{h}}(z)$	$\mathrm{ML^{-1}T^{-2}}$	$\sigma_{h}(z)/(\rho_{\mathrm{s}}aH)$ $\sigma_{\mathrm{h}}(z)/(\rho_{\mathrm{s}}az)$
Independent variables	Height of cylinder	H	L	Repeated
	Diameter of cylinder	D	L	D/H
	Depth of soil in front of cylinder	h	L	h/H
	Wall thickness of cylinder	t	L	t/H
	Density of cylinder	ρ	$\mathrm{ML^{-3}}$	ρ/ρ_{s}
	Young's modulus of cylinder	E	$\mathrm{ML^{-1}T^{-2}}$	$E/(\rho_{\mathrm{s}}aH)$
	Poisson's ratio of cylinder	ν	—	ν
	Density of water	ρ_{w}	$\mathrm{ML^{-3}}$	$\rho_{\mathrm{w}}/\rho_{\mathrm{s}}$
	Thickness of soil deposit	T	L	T/H
	Density of soil deposit	ρ_{s}	$\mathrm{ML^{-3}}$	Repeated
	Young's modulus of soil deposit	E_{s}	$\mathrm{ML^{-1}T^{-2}}$	$E_{\mathrm{s}}/(\rho_{\mathrm{s}}aH)$
	Poisson's ratio of soil deposit	ν_{s}	—	ν_{s}
	Apparent cohesion or undrained shear strength	C, C_{U}	$\mathrm{ML^{-1}T^{-2}}$	$c/(\rho_{\mathrm{s}}aH)$ or $c_{\mathrm{U}}/(\rho_{\mathrm{s}}aH)$
	Tangent of angle of shearing resistance	$\tan\varphi$	—	$\tan\varphi$
	Interface friction between soil and wall	$\tan\varphi^{*}$	—	$\tan\varphi^{*}$
	Acceleration of inertial force field	a	$\mathrm{LT^{-2}}$	Repeated
	Uniformly distributed load	q	$\mathrm{ML^{-1}T^{-2}}$	$q/(\rho_{\mathrm{s}}aH)$
	Line load	F	$\mathrm{MT^{-2}}$	$F/(\rho_{\mathrm{s}}aH^{2})$
	Horizontal distance from the front face of wall	x	L	x/H
	Depth below ground surface	z	L	z/H

Note: "R" denotes repeated variable (Butterfield, 1999).

Also, the lateral earth pressure, $\sigma_h(z)$, acting on the wall at any depth z can be expressed in terms of its independent DGs as follows:

$$\sigma_h(z)/(\rho_s az) = \Phi_4\{D/H, h/H, t/H, \rho/\rho_s, E/(\rho_s aH), \nu, T/H, E_s/(\rho_s aH), \nu_s, c/(\rho_s aH), \tan\varphi, \rho_w/\rho_s, \tan\varphi^*, q/(\rho_s aH), F/(\rho_s aH)\}, z/H \quad (4a)$$

But, for a given wall type (material) and geometry, $\sigma_h(z)$ acting at any depth z, may be simplified as follows:

$$\sigma_h(z)/(\rho_s az) = \Phi_5\{\delta_h/H, c/(\rho_s aH), \tan\varphi, q/(\rho_s aH), F/(\rho_s aH)\}, z/H \quad (4b)$$

It should be noted that the left-hand side of Equations (4a) and (4b) is in fact a dimensionless lateral earth pressure coefficient.

Since the acceleration in any centrifuge model test will increase from 1g (i.e., 9.81 m/s^2) to N times g (i.e., Ng), it is of great interest to substitute a=Ng in the above equations. For a given soil, a given wall and given applied external loads in centrifuge tests, DGs, such as t/H, ρ/ρ_s, ν, ρ_w/ρ_s, T/H, ν_s, $E/(\rho_s NgH)$, $E_s/(\rho_s NgH)$, $q/(\rho_s NgH)$ and $F/(\rho_s NgH^2)$, can be regarded as constants. Thus, Equations (2), (3) and (4) can be greatly simplified into as follows:

$$\delta_h(z)/H = \Phi_6\{D/H, h/H, \tan\varphi, \tan\varphi^*\} \quad (5)$$

$$s(x)/H = \Phi_7\{D/H, h/H, c/(N\rho_s gH)\tan\varphi, \tan\varphi^*\} \quad (6)$$

$$\sigma_h(z)/(N\rho_s gz) = \Phi_8\{\sigma_h/H, c/(N\rho_s gH), \tan\varphi, \tan\varphi^* z/H\} \quad (7)$$

2 Centrifuge model tests

2.1 Test program

The objectives of the centrifuge model tests are to investigate the governing factors and their relative importance to stability and deformation mechanisms of a quay wall. The design of the centrifuge models was primarily in reference to the current practice in China. Disturbed soft clay samples were taken from a proposed construction site for use in the model tests. The cylinder, by which the quay wall was constructed in-situ, is 18 m in diameter and 24 m in height.

By means of the results from the dimensional analysis expressed in Equations (5), (6) and (7), for a given soil type, the ratio of the embedded depth to wall height (h/H), the ratio of the diameter of the cylinder to the wall height (D/H), and the interface friction between the soil and the quay wall ($\tan\varphi^*$) become the three obvious DGs for investigation. With these in mind, three series of centrifuge model tests were planned. Details of the tests are given in Table 2. In the first series, D, H and $\tan\varphi^*$ were kept constant but h varied from 0 to 75 mm (model scale), which gave rise to a range of h/H varying from 0 to 0.5. In the second series, three diameters of cylinders, ranging from 85 mm to 160 mm (model scale) were used, but all the other variables were kept the same. This resulted in three different D/H values, 0.57, 0.73 and 1.07. In the last series, all variables were kept the same among the three planned tests, except three different interface characteristics were adopted, leading to three values of $\tan\varphi^*$ (0.36, 0.49 and 0.58). As shown in the Table, 7 centrifuge tests were conducted following a three series test plan.

To simulate three different diameters of cylinders in a model box 685 mm long, 350 mm wide and 450 mm deep, the designed acceleration in the centrifuge was 164g. Thus, the performance of each model at the acceleration of 164g is regarded as the reference case, although the actual maximum acceleration used ranging from 165g to 175g.

2.2 Model preparations and test procedures

Bottomless model cylinders made of Perspex tubes were used to simulate the quay wall as shown in Figs. 2a and 2b. The height of the three cylinders used in each test was 150 mm. Depending on the test series (see Table 2), three different types of cylinders with external diameters ranging from 85 mm, 110 mm to 160 mm were adopted in the different tests. The walls of the cylinders were roughened by rubbing them with abrasive cloth to different degrees for studying the influence of interface wall frictions. If required, the roughness of the wall was further enhanced by adhering a layer evenly distributed sand grains to the wall surface with epoxy. The actual friction coefficient between the soil and the cylinder wall was determined by direct shear tests in the laboratory. The measured interface angles were 19.8°, 26.1° and 30.1° for three different surface conditions of no special treatment, rubbed with an abrasive cloth and glued with a thin layer of sand, respectively.

Three soil layers were placed in each centrifuge model (see Fig. 2a). The bottom layer, i.e., the bearing stratum of the quay wall, was composed of dense medium-course sand. It had the maximum dry density of 1670 kg/m^3 and the minimum dry density of 1340 kg/m^3. This layer was prepared by running the sand through a

Table 2 Details of centrifuge test series

Series	Model No.	*D*/m	*H*/m	*h*/m	*h*/*H*	*D*/*H*	tanφ*
	M11	0.110	0.150	0.000	0.00	0.73	0.49(26°)
1. *h*/*H*	M12	0.110	0.150	0.045	0.30	0.73	0.49(26°)
	M13	0.110	0.150	0.075	0.50	0.73	0.49(26°)
	M15	0.085	0.150	0.045	0.30	0.57	0.49(26°)
2. *D*/*H*	M12	0.110	0.150	0.045	0.30	0.73	0.49(26°)
	M14	0.160	0.150	0.045	0.30	1.07	0.49(26°)
	M17	0.110	0.150	0.045	0.30	0.73	0.36(20°)
3. tanφ*	M12	0.110	0.150	0.045	0.30	0.73	0.49(26°)
	M18	0.110	0.150	0.045	0.30	0.73	0.58(30°)

Note: thickness of all cylinders is 0.005 m.

hole of a sand hopper from at a fixed height into the model container, producing a uniform bottom stratum with a dry density of 1640 kg/m^3.

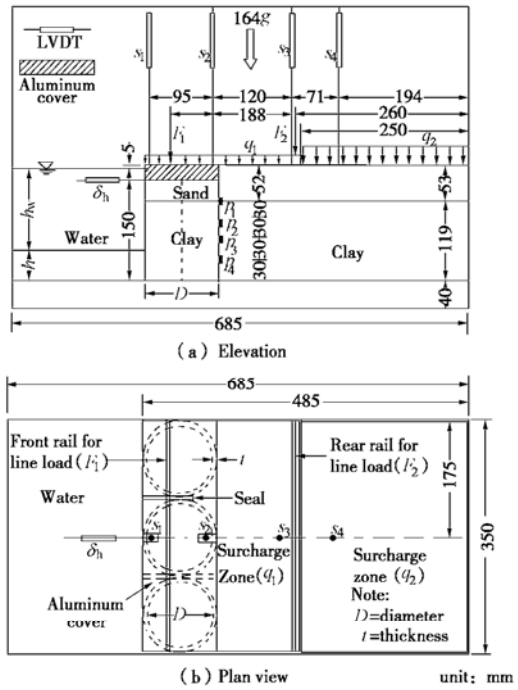

Fig. 2 Model set-up

The middle layer, placed above the sand stratum, was made of gray clay, which had a liquid limit and plastic limit of 36% and 20%, respectively. The clay stratum was prepared by consolidating slurry in two stages. In the first stage, the clay slurry was consolidated into a block of soil at 164*g* in the centrifuge. Upon completion of this stage of consolidation, the model cylinders were pushed through the clay and rested on the dense sand stratum at one gravity. Then, 50 kg of gravel fill was placed evenly on the top of the clay surface to impose a surcharge load. Subsequently, the second stage of consolidation was carried out with the surcharge load from 1*g* to 175*g* for 3 hours and at 175*g* for 2.5 hours in order to improve the shear strength of the soft clay. At 175*g*, the surcharge pressure was 365 kPa. After these two stages of consolidation and removal of the surcharge load, the undrained shear strength (c_u) profile of the clay deposit for each test was measured by means of a pocket cone penetrometer at one gravity (see Fig. 3). Due to the loading and unloading preparation procedures adopted, the upper clay was overconsolidated and the lower soil was normally consolidated, as required for simulating the in-situ desiccation effects on shear strength of the soft clay. Thus, the measured profiles can be divided into two zones. At shallow depth, i.e., less than 80 mm deep, the measured undrained shear strength decreases with depth, as a result of the reduction of the overconsolidation ratio with depth. At deeper layers, i.e., at 80 mm or deeper, the measured c_u profile increases with depth due to an increase in confining stresses. The variations of undrained shear strength with depth among different models are reasonably consistent and the magnitude of undrained shear strength is generally representative of the soft to medium clay stratum in the field.

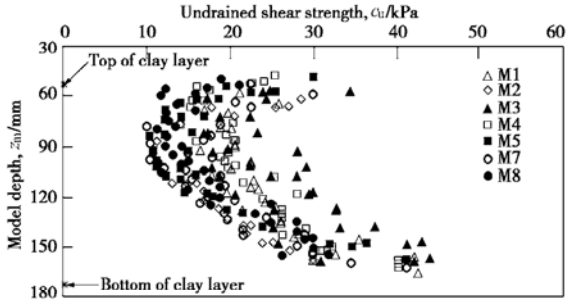

Fig. 3 Profiles of undrained shear strength

The final preparation work of the centrifuge model was to fill a layer of gravel with particle sizes ranging

from 2 mm to 10 mm as a surcharge over the clay stratum and to excavate the clay block in front of the quay wall (see Fig. 2a). The cylinders were filled and compacted with the same sand as that in the bearing stratum. To increase the rigidity of each cylinder, a perforated 22 mm thick aluminum plate was used to "brace" the cylinder at the top (see Fig. 2b). The retained height at the top of the cylinder was 172 mm (see Fig. 2a).

To simulate the influence of concrete pavement rigidity and surface loads, one 1.5 mm-thick aluminum plate and another 1.2 mm-thick tin sheet were placed on top of the gravel for modeling in-situ uniformly distributed loads, i.e., q_{1max}=7 kPa and q_{2max} =14 kPa at 164g, respectively and two miniature rails were used to simulate concentrated line loads from the weight of cargo, cargo handling and hauling equipment, giving rise to F_{1max}=F_{2max}=2.1 kN/m at 164g. All the centrifuge model tests were carried out in Nanjing Hydraulic Research Institute in China.

2.3 Instrumentation

In order to monitor the performance of the model quay wall, four linear variable differential transformers (LVDTs), s_1, s_2, s_3 and s_4, were mounted along the centerline of the model container to measure the vertical settlements at various distances from the quay wall (see Fig. 2a). s_1 and s_2 were used to monitor the settlements of the cylinder and s_3 and s_4 were used to measure the settlements of the backfill behind the quay wall. In addition, a fifth LVDT, i.e., δ_h, was used to record the horizontal displacement at the top of the quay wall.

To study the distributions of the lateral earth pressures, four miniature earth pressure cells, p1, p2, p3 and p4, were installed along the back of the quay wall at various depths (see Fig. 2a). They were located at 0.35H, 0.55H, 0.75H and 0.95H, where H is 150 mm, from the ground surface.

3 Interpretation of test results

3.1 Typical deformation mode of the quay wall

Since it is extremely difficult to install any submerged instrumentation to measure horizontal displacement of the lower part of the embedded cylinders in the model, there are not enough data about the horizontal movement of the cylinder to describe its lateral displacement behavior in detail. However, the general displacement mode can be characterized in terms of the normalized horizontal displacement at the top front of the cylinder, δ_h/H, and the wall tilt, $(s_1-s_2)/d_{s1\text{-}s2}$, where $d_{s1\text{-}s2}$ is the distance between locations s_1 and s_2 (refer to Figs. 2a and 2b).

Fig. 4 shows the development of normalized vertical settlements at four locations (i.e., s_1, s_2, s_3 and s_4) whereas Fig. 5 depicts the normalized horizontal displacement at the top of the wall (δ_h) and the wall tilt (i.e., $(s_1-s_2)/d_{s1\text{-}s2}$), where $d_{s1\text{-}s2}$ is the distance between s_1 and s_2, with normalized acceleration for a typical model test, M4. It can be seen that the magnitude of the vertical movements (i.e., the heave at s_1 and s_2 but the settlement at s_3 and s_4) and the forward horizontal displacement (δ_h) of the wall increases with the normalized acceleration. The heave and forward horizontal displacement at the top of the wall and the settlement of the soil behind it seems to indicate a complex and combined translational and counter clockwise rotational motion (or tilt) of the quay wall, as a result of the increasing body weight due to the increased gravity. Similar behavior was also observed in other tests.

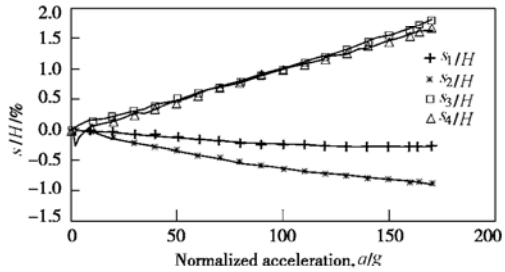

Fig. 4 Variations of settlement with acceleration (M4)

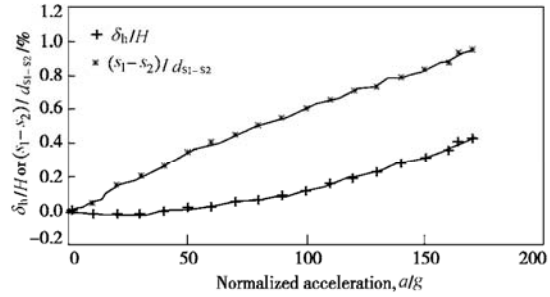

Fig. 5 Variations of horizontal displacement and rotation with acceleration (M4)

3.2 Effects of h/H, D/H, and $\tan\varphi^*$ on the horizontal displacement of the quay wall

From Equation (5), it is obvious that the horizontal displacement at the top of the quay wall is a function of

three DGs, h/H, D/H and $\tan\varphi^*(=f^*)$ for a given soil. Fig. 6 shows the variations in the normalized horizontal displacement at the top of the wall (δ_h/H) with the three DGs at 164g. In the test series with different h/H values (see Table 2), δ_h/H decreases significantly with an increase in the h/H ratio. An excessive lateral movement occurs when there is no embedment in front of the quay wall (i.e., h/H = 0). However, as the depth of the soil increases, the lateral movement of the wall is greatly reduced and it even approaches zero when h/H is close to 0.5. This suggests that an increase in the soil embedment depth in front of the wall will be a very effective measure in reducing lateral wall displacement.

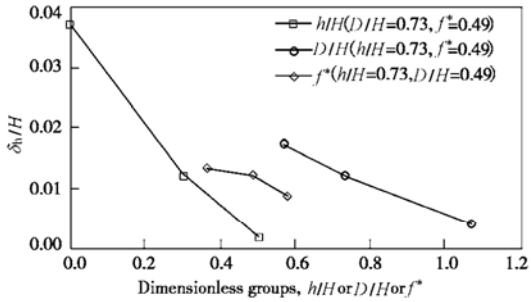

Fig. 6 Variations of normalized horizontal displacement with DGs at 164g

In the test series with different D/H values (see Table 2), an approximate linear relationship between δ_h/H and D/H can be found in Fig. 5. As expected, δ_h/H decreases as D/H increases, resulting from an increase in the base shearing resistance and lateral stability for a given wall height. In the figure, the influence of the interface friction coefficient, $f^*=\tan\varphi^*$, on δ_h/H can also be identified. As f^* increases, the lateral active earth pressure decreases whereas the passive earth pressure increases, leading to a reduction in the horizontal displacement of the wall. The results of deformation characteristics at 164g for all three test series are summarized in Table 3.

In order to investigate the relative importance (or sensitivity) of the three DGs to the horizontal displacement of the wall quantitatively, a multiple linear regression analysis (Ang & Tang, 1975) was carried out. The results of the analysis are given in the following equation:

$$\frac{\delta_h}{H}=0.055-0.050\frac{h}{H}-0.025\frac{D}{H}-0.020\tan\varphi^* \quad (8)$$

It should be noted that since the data for M1 is estimated by interpolations, they are not included in the regression analysis. By comparing the coefficients in Equation (8), it is obvious that the horizontal wall displacement is most sensitive to the h/H ratio since it has the largest regression coefficient. In fact, the horizontal wall displacement is 50% less sensitive to D/H than to h/D and it is most insensitive to interface friction between the soil and the wall among the three DGs.

3.3 Distributions of dimensionless earth pressure along the back of the quay wall

Based on the results from DA given by Equations (4) and (7), for the given soil and test conditions, the dimensionless variable, $\sigma_h(z)/(\rho_s az)$, which essentially is a lateral earth pressure coefficient, should be a function of δ_h/H. Figs. 7 and 8 show the variations of dimensionless lateral earth pressure with normalized horizontal displacement for a smooth (M7) and a rough (M8) wall, respectively. It can be seen from Fig. 7 that when the quay wall and soil are loaded by an increasing centripetal acceleration (a), the wall moves away from the retained soil and $\sigma_h(z)/(\rho_s az)$ at each pressure cell changes from its initial value. For pressure cell p1 at z/H= 0.35, $\sigma_h(z)/(\rho_s az)$ appears to reach a peak value of 0.93 at δ_h/H about equal to 0.2% δ_h/H and then reduces

Table 3 Summary of displacement characteristics at 164g

Series	Model No.	DGs			Dependent variables (characteristic of displacement)					$(s_1-s_2)/d_{s1\text{-}s2}$/%
		h/H	D/H	$\tan\varphi^*$	δ_h/H/%	s_1/H/%	s_2/H/%	s_3/H/%	s_4/H/%	
	M1	0.00	0.73	0.49	3.70					
1.h/H	M2	0.30	0.73	0.49	1.23	−0.17	−1.29	2.36	1.63	1.78
	M3	0.50	0.73	0.49	0.20	−0.45	−0.73	1.81	1.80	0.43
	M5	0.30	0.57	0.49	1.73	−0.14	−1.06	2.47	1.15	1.97
2.D/H	M2	0.30	0.73	0.49	1.23	−0.17	−1.29	2.36	1.63	1.78
	M4	0.30	1.07	0.49	0.41	−0.27	−0.86	1.74	1.62	0.93
3. $\tan\varphi^*$	M7	0.30	0.73	0.36	1.35	−0.02	−1.12	2.07	1.49	1.74
	M2	0.30	0.73	0.49	1.23	−0.17	−1.29	2.36	1.63	1.78
	M8	0.30	0.73	0.58	0.87	−0.23	−0.61	1.75	1.05	0.59

Note: (1). δ_h— forward movements being taken as positive; s_1, s_2, s_3 and s_4—downward settlements being taken as positive. (2). The distance between s_1 and s_2 is 95 mm, and that between s_1 and s_3 is 215 mm; but for M15, the distance between s_1 and s_2 is 70 mm only. (3). The data of δ_h for M11 is obtained by interpolating.

toward an approximate constant value of 0.75 at about 0.6% or larger. For p3 at z/H = 0.75, however, $\sigma_h(z)/(\rho_s az)$ increases with the g-level initially and it reaches a constant value of 1.0 at δ_h/H=0.3% or larger. Similar behavior is observed at p4 (i.e., z/H = 0.95) and the dimensionless earth pressure coefficient reaches an almost constant value of 0.93 at δ_h/H= 0.3% or larger. However, the behavior at p2 (i.e., z/H = 0.55) is very different from the other three. $\sigma_h(z)/(\rho_s az)$ is very high initially, probably due to the low shear strength of the clay at the location of p2, i.e., z = 82 mm (see Fig. 3). As δ_h/H increases with the centripetal acceleration, the dimensionless earth pressure coefficient decreases between but at a much reduced rate and it finally reaches an ultimate value of 0.8 at δ_h/H=1.35%. All four earth pressure cells show consistent dimensionless earth pressure coefficients varying from 0.75 to 1.0 and they remain almost constant at large δ_h/H values, typically 0.4%, suggesting that the wall reaches the "active" state.

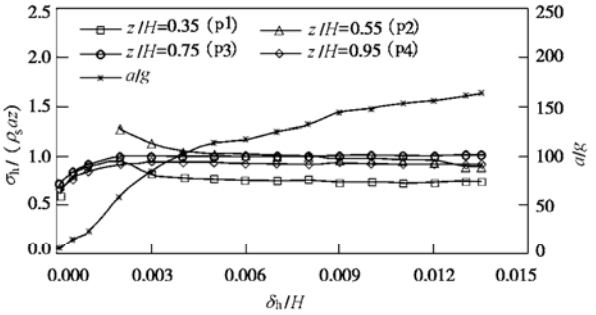

Fig. 7 Variations of dimensionless earth pressure with normalized horizontal displacement (M7)

Fig. 8 depicts the development of $\sigma_h(z)/(\rho_s az)$ with δ_h/H at three locations of a rough wall (M8). Though p1 ceased functioning during the test, it can be seen that the retained soil reaches the active state at δ_h/H=0.4%. The measured active earth pressure coefficients are 1.0 for p2 and 0.9 for p3 and p4. The small difference between the measured coefficients in M7 and M8 tests suggests that the roughness of the wall has a limited influence on the lateral earth pressures and hence it has little influence on the stability of this type of quay wall.

Based on the total stress analysis, Rankine's active lateral earth pressure, p_a, acting on the wall can be calculated using the following equation (Padfield and Mair, 1984):

$$p_a = K_a\sigma_v - 2c_u\sqrt{K_a(1+\frac{c_w}{c_u})} \quad (9)$$

where c_w is wall adhesion, σ_v is total vertical stress and K_a=1.0 for ϕ_u=0.

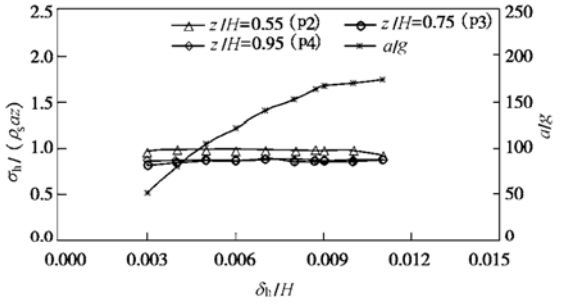

Fig. 8 Variations of dimensionless earth pressure with normalized horizontal displacement (M8)

Using the above equation, the calculated distributions of the active lateral earth pressure with depth for three assumed c_w cases are compared with measured values at 164 g and they are shown in Fig. 9 and Fig. 10 for M7 and M8, respectively. It can be seen that the measured values are generally consistent with computed results, irrespective of the wall texture (roughness), indicating that the clay behind the wall essentially behaves in an undrained manner. The influence of the wall texture on the lateral earth pressure is not significant for this type of quay wall. Rankine earth pressure theory seems to be able to capture the behavior of the quay wall.

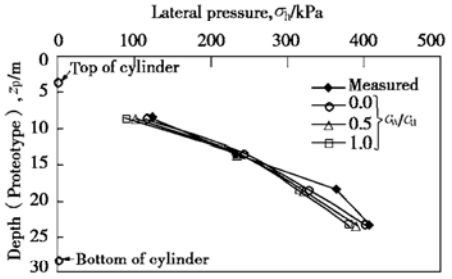

Fig. 9 Distribution of lateral pressures along the back wall of cylinder (M7)

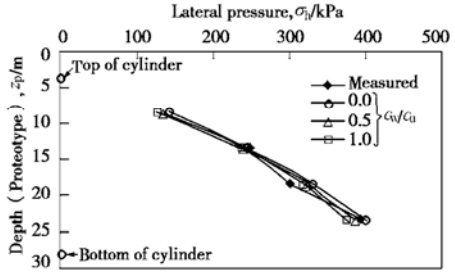

Fig. 10 Distribution of lateral pressures along the back wall of cylinder (M8)

4 Conclusions

(1) By dimensional analysis, the dimensionless

groups (DGs), which determine the performance of the soil-structure interaction in an embedded quay wall using large-diameter bottomless cylinders, are identified. In centrifuge tests using the same model soil and model wall materials, the performance of quay wall is mainly governed by three dimensionless groups, i.e., the diameter to the height of the cylinder, (D/H), the depth of the soil in front of the wall to the height of the cylinder, (h/H), and the interface wall friction between the soil and the wall, ($\tan\varphi^*$).

(2) Based on 7 centrifuge model tests, a similar deformation mechanism is observed, in which the upper part of the wall tilts away from the retained soil and the ground behind it settles. As expected, the larger the values of h/H, D/H and $\tan\varphi^*$, the smaller the horizontal displacement, (δ_h/H), the wall tilt ($(s_1-s_2)/d_{s1\text{-}s2}$), and the ground settlement (s_3/H).

(3) From multiple linear regression analysis, it is found that the relative horizontal displacement of the quay is 50% more sensitive to the ratio of h/H than to D/H. Relatively, the influence of the texture (roughness) of the wall (i.e., $\tan\varphi^*$) on the horizontal displacement is limited.

(4) From the measured lateral earth pressures in the centrifuge model tests, it appears that the retained clay behind the quay wall reaches its active state when δ_h/H approaches 0.4% in all 7 tests. Since the influence of the roughness/adhesion of the wall is limited, the measured lateral earth pressures can be predicted by using Rankine's active earth pressure theory with the undrained assumption in the short-term.

5 Acknowledgements

This research project is supported by research grant HKUST6025/01E provided by the Research Grants Council of the HKSAR, and the two research funds, GCG99/00.EG01 and OAP98/99.EG01, provided by the Geotechnical Consulting Group (Asia) Ltd and Ove Arup & Partners, respectively.

References:

[1] ANG A H S, TANG W H. Probability Concepts in Engineering Planning and Design. Volume 1, Basic principles[M]. John Wiley & Sons, New York, 1975.

[2] BUTTERFIELD R. Dimensional analysis for geotechnical engineers, Geotechnique, 1999, **49**(3): 357 - 366.

[3] LIU JQ. Deformation of large-diameter cylindrical buried structures[J]. Chinese Journal of Geotechnical Engineering, 1994, **16**, (2): 64 - 72. (in Chinese)

[4] PADFIELD C J, MAIR R J. Design of retaining walls embedded in stiff clay[R]. CIRIA Report 104. Construction Industry Research and Information Association, 1984.

[5] SEDOV L I. Similarity and Dimensional Methods in Machanics[M]. 10th Edition. CRC Press, New York, 1993.

[6] TSINKER G P. Handbook of Port and Harbor Engineering: Geotechnical and Structural Aspects[M]. ITP International Thomson Publishing, CHAPMAN & Hall Press, New York, 1997.

[7] ZHOU X R, LIU J L. Application of large-diameter cylinders to port engineering and considerations for their structure designs and computations[J]. Chinese Port Engineering, 1995: 1 - 10. (in Chinese)